JOURNAL OF GUIDANCE, CONTROL, AND DYNAMICS
Vol. 37, No. 3, May–June 2014

Engineering Notes

Analytical Guidance Solutions for Spacecraft Planar Rephasing via Input Shaping

Riccardo Bevilacqua*
Rensselaer Polytechnic Institute, Troy, New York 12180

DOI: 10.2514/1.G000008

I. Introduction

Autonomy in spacecraft guidance, navigation, and control (GNC) is crucial to enable, for example, proximity operations as those targeted by NASA.† Autonomous GNC demands for analytical or semi-analytical solutions to be used in missions where computation capabilities or ground communications may be extremely limited.

With the intent to contribute to the field of autonomous spacecraft GNC, this Note focuses on the derivation of new analytical guidance solutions for spacecraft planar rephasing, considering realistic, along-track, continuous, on–off control only. The along-track, continuous, on–off control restriction reflects physical spacecraft layouts, where just a few orbital control engines may be available and pointed in a predetermined direction, as presented in [1,2]. In addition, on–off continuous thrust modeling in spacecraft orbital guidance relates to recent research and development of continuous and low-thrust engines, as described, for example, in [3,4].

Input-shaping theory, presented in [5–12], and the Hill–Clohessy–Wiltshire linear equations of spacecraft relative motion, described in [13,14], are combined to obtain new analytical guidance solutions to the problem of short-distance (a few kilometers) planar spacecraft rephasing. A satellite starting from a circular orbit or a slightly eccentric one can be rephased to a new polar angle on the same orbit. In particular, the final state can be a new position along the original orbit, if starting from circular motion, or a closed relative path with respect to a chosen point, if starting from an eccentric orbit. The rephasing solutions proposed in this Note are open-loop maneuvers going from an equilibrium configuration to a new equilibrium configuration, where equilibrium indicates a nondrifting condition with respect to the final desired polar angle.

The original contribution of this Note consists of new analytical orbital guidance solutions, obtained using input shaping. Input shaping is commonly used for vibration suppression of flexible structures, and it is here proposed for the first time as an orbital guidance design tool, enabling the modeling of realistic orbital control engines.

Received 30 April 2013; revision received 14 October 2013; accepted for publication 26 November 2013; published online 20 February 2014.

*Assistant Professor, Department of Mechanical, Aerospace, and Nuclear Engineering, 110 8th Street. Member AIAA.

†Data available online at http://ssco.gsfc.nasa.gov/about.html [retrieved 28 September 2013].

II. Analytical Solutions Derivation for Spacecraft Rephasing

A. Spacecraft Relative Motion Dynamics and Input-Shaping Control

Spacecraft relative motion dynamics is used to model how a space vehicle moves with respect to the final desired rephase location. Thus, the rephasing target point is chosen as the origin of the local vertical/local horizontal (LVLH) reference frame. This frame is defined with the x axis pointing from Earth to the reference satellite in circular orbit (virtual or real), y points along the track (direction of motion), and z completes the right-handed frame. In LVLH, the in-plane, linearized dynamics of spacecraft relative motion with along-track control only, is given by Eq. (1), found in [13,14]:

$$\dot{\boldsymbol{x}} = \underline{\underline{A}}\boldsymbol{x} + \underline{\underline{B}}\boldsymbol{u}, \qquad \underline{\underline{A}} = \begin{bmatrix} 0 & 0 & 1 & 0 \\ 0 & 0 & 0 & 1 \\ 3\omega^2 & 0 & 0 & 2\omega \\ 0 & 0 & -2\omega & 0 \end{bmatrix}, \qquad \underline{\underline{B}} = \begin{bmatrix} 0 \\ 0 \\ 0 \\ 1 \end{bmatrix},$$
$$\omega = \frac{2\pi}{T}, \qquad \boldsymbol{x} = [x \quad y \quad \dot{x} \quad \dot{y}]^T, \qquad \boldsymbol{u} = u_y \tag{1}$$

where T is the orbital period. The analytical solution to Eq. (1), with constant control $u_y = \bar{u}$, and initial condition at t_0, is obtained as

$$\boldsymbol{x}(t) = \underline{\underline{\Phi}}(t)\boldsymbol{x}(t_0) + \underline{\underline{\Psi}}(t)\bar{u},$$
$$\underline{\underline{\Phi}}(t) = \begin{Bmatrix} 4-3\cos(\alpha) & 0 & \sin(\alpha)/\omega & [-2\cos(\alpha)+2]/\omega \\ 6\sin(\alpha)-6\alpha & 1 & [2\cos(\alpha)-2]/\omega & [-3\alpha+4\sin(\alpha)]/\omega \\ 3\omega\sin(\alpha) & 0 & \cos(\alpha) & 2\sin(\alpha) \\ 6\omega\cos(\alpha)-6\omega & 0 & -2\sin(\alpha) & -3+4\cos(\alpha) \end{Bmatrix},$$
$$\underline{\underline{\Psi}}(t) = \begin{Bmatrix} 2[\sin(\alpha)+\alpha]/\omega^2 \\ -(1/2)[-8+3\alpha^2+8\cos(\alpha)]/\omega^2 \\ -2[-1+\cos(\alpha)]/\omega \\ -[3\alpha-4\sin(\alpha)]/\omega \end{Bmatrix}$$
$$\alpha = \omega(t-t_0) \tag{2}$$

Input shaping is based on the concept of providing and then removing energy to/from an oscillatory system. A train of specific impulses is convoluted with a control signal to achieve the desired final state with minimal residual vibration, as described in [12]. In this Note, the control signal to be shaped is chosen as a bang–bang profile of amplitude $\bar{u}$, and a three-impulse shaper is proposed, as described in Eq. (3):

$$u_y = A_1 f_{t_1} + A_2 f_{t_2} + A_3 f_{t_3}, \qquad A_1 = \frac{1}{4}, \qquad A_2 = \frac{1}{2}, \qquad A_3 = \frac{1}{4}$$
$$f_{t_1} = \begin{cases} \bar{u}\,\text{sign}[y_{\text{fd}} - y(t_0)], & \text{if } t \le t^*/2 \\ -\bar{u}\,\text{sign}[y_{\text{fd}} - y(t_0)], & \text{if } t^*/2 < t \le t^* \\ 0, & \text{if } t > t^* \end{cases},$$
$$f_{t_2} = f_{t_1}(t-\Delta t), \qquad f_{t_3} = f_{t_1}(t-2\Delta t)$$
$$t^* = \sqrt{2|y_{\text{fd}} - y(t_0)|/\bar{u}} \tag{3}$$

where y_{fd} indicates the final desired along-track position. The impulses A_i are given in [12], respectively, by $1/(1+K)^2$, $2K/(1+K)^2$, and $K^2/(1+K)^2$, with $K = \exp[-\zeta\pi/(1-\zeta^2)^{1/2}]$, and ζ indicates the damping ratio of the given dynamic system. For this Note, $\zeta = 0$, leading to the A_i values in Eq. (3). The effect of the coasting phases Δt is explained in the following sections.

B. Analytical Solution for Initial Circular Orbit

The direct application of Eq. (3) on Eq. (1), starting from the LVLH circular orbit [i.e., $\boldsymbol{x}(t_0) = (\,0 \quad y_0 \quad 0 \quad 0\,)^T$ and considering a variable Δt], results in the following expression for the final state:

$$
\begin{aligned}
&c = \cos(\dots)\\
&e_{\text{rel}} = 0.5\sqrt{2}\frac{\bar{u}}{\omega^2}\sqrt{\begin{array}{l} 6c\left(\tfrac{2}{3}\alpha_2\right) - 4c\left(-\tfrac{1}{3}\alpha_2 + 2\omega\Delta t\right) - 4c\left(2\omega\Delta t + \tfrac{1}{3}\alpha_2\right) + c\left(-\tfrac{2}{3}\alpha_2 + 2\omega\Delta t\right) + \\ +4c\left(\omega\Delta t - \tfrac{2}{3}\alpha_2\right) - 16c\left(\tfrac{1}{3}\alpha_2 + \omega\Delta t\right) - 24c\left(\tfrac{1}{3}\alpha_2\right) - 16c\left(\omega\Delta t - \tfrac{1}{3}\alpha_2\right) + \\ +18 + c\left(2\omega\Delta t + \tfrac{2}{3}\alpha_2\right) + 6c(2\omega\Delta t) + 24c(\omega\Delta t) + 4c\left(\omega\Delta t + \tfrac{2}{3}\alpha_2\right) \end{array}}\\
&\alpha_2 = \omega\sqrt{\frac{3y_{\text{fd}} - 3y_0}{\bar{u}}}
\end{aligned}
\tag{8}
$$

$$
\begin{aligned}
&s = \sin(\dots)\\
&c = \cos(\dots)\\
&x_f = x(t^* + 2\Delta t)\\
&\quad = \frac{\bar{u}}{\omega^2}\begin{bmatrix} -2s(0.5\alpha_1 + \omega\Delta t) - s(0.5\alpha_1 + 2\omega\Delta t) + s(\alpha_1 + \omega\Delta t) + \\ +0.5s(\alpha_1 + 2\omega\Delta t) - s(0.5\alpha_1) + 0.5s(\alpha_1) + 0.5s(2\omega\Delta t) \\ +s(\omega\Delta t) \end{bmatrix}\\
&y_f = y(t^* + 2\Delta t)\\
&\quad = \frac{\bar{u}}{\omega^2}\begin{bmatrix} -2c(0.5\alpha_1 + 2\omega\Delta t) - 4c(0.5\alpha_1 + \omega\Delta t) + 2c(\alpha_1 + \omega\Delta t) \\ +c(\alpha_1 + 2\omega\Delta t) - 2c(0.5\alpha_1) + c(\alpha_1) + c(2\omega\Delta t) + \\ +2c(\omega\Delta t) - 0.5y_0(\omega^2/\bar{u}) + \\ +1.5y_{\text{fd}}(\omega^2/\bar{u}) + 1 \end{bmatrix}\\
&\dot{x}_f = \dot{x}(t^* + 2\Delta t)\\
&\quad = \frac{\bar{u}}{\omega}\begin{bmatrix} -c(0.5\alpha_1 + 2\omega\Delta t) - c(0.5\alpha_1 + \omega\Delta t) + c(\alpha_1 + \omega\Delta t) + \\ +0.5c(\alpha_1 + 2\omega\Delta t) - c(0.5\alpha_1) + 0.5c(\alpha_1) + \\ +c(\omega\Delta t) + 0.5c(2\omega\Delta t) + 0.5 \end{bmatrix}\\
&\dot{y}_f = \dot{y}(t^* + 2\Delta t)\\
&\quad = \frac{\bar{u}}{\omega}\begin{bmatrix} 4s(0.5\alpha_1 + \omega\Delta t) + 2s(0.5\alpha_1 + 2\omega\Delta t) - 2s(\alpha_1 + \omega\Delta t) + \\ -s(\alpha_1 + 2\omega\Delta t) + 2s(0.5\alpha_1) - s(\alpha_1) - s(2\omega\Delta t) - 2s(\omega\Delta t) \end{bmatrix}\\
&\alpha_1 = \omega\sqrt{\frac{2(y_{fd} - y_0)}{\bar{u}}}
\end{aligned}
\tag{4}
$$

The resulting motion after $t_f = t^* + 2\Delta t$ is an equilibrium, because the condition $\dot{y}_f = -2\omega x_f$ is satisfied, guaranteeing a closed, nondrifting relative orbit (see [13,14]). Also, the center of the ellipse representing the final relative orbit is given by the following formula from [15], applied on Eq. (4):

$$\bar{x} = 4x_f + 2\dot{y}_f/\omega = 0 \quad \bar{y} = y_f - 2\dot{x}_f/\omega = -0.5y_0 + 1.5y_{\text{fd}} \tag{5}$$

The resulting trajectory has the center located at the desired along-track location y_{fd}, if a new desired virtual location y'_{fd} [given in Eq. (6)] is selected, to be used in Eq. (3). In fact, replacing y_{fd} with y'_{fd} in Eq. (5), the expression for $\bar{y}$ reduces to y_{fd}:

$$y'_{\text{fd}} = (2/3)y_{\text{fd}} + (1/3)y_0 \rightarrow \bar{y} = y_{\text{fd}} \tag{6}$$

The relative eccentricity, representing the physical dimension of the obtained closed orbit, is given by [15] in the following formula:

$$e_{\text{rel}} = \sqrt{a^2 + (b/2)^2}, \qquad a = x_f - \bar{x}, \qquad b = y_f - \bar{y} \tag{7}$$

Substituting Eqs. (4–6) into Eq. (7), the direct dependency of e_{rel} from Δt is obtained:

If $\Delta t = 0.5T = \pi/\omega$, the resulting relative eccentricity is zero, and the final state is $\boldsymbol{x}(t_f) = [\,0 \quad y_{\text{fd}} \quad 0 \quad 0\,]^T$, that is, the spacecraft is on the same initial orbit, at the desired along-track position. Equation (8) cannot be solved in closed form in terms of Δt, when a desired e_{rel} is given. Nevertheless, its derivative with respect to Δt can be computed [Eq. (9)], showing maximum relative eccentricity for $\Delta t = k2\pi/\omega$, $k = 1, 2, \dots$ and zero relative eccentricity for $\Delta t = k\pi/\omega$, $k = 1, 2, \dots$:

$$
\begin{aligned}
\frac{\partial e_{\text{rel}}}{\partial(\Delta t)} &= -\frac{8\bar{u}^2[\cos(\omega\Delta t/2)]^3\sin(\omega\Delta t/2)\eta}{\omega^3\sqrt{(\bar{u}^2/\omega^4)[\cos(\omega\Delta t/2)]^4\eta}},\\
\eta &= \left\{\left[\cos\left(\frac{\omega}{12}\sqrt{-\frac{12y_0 - 12y_{\text{fd}}}{\bar{u}}}\right)\right]^2 - 1\right\}^2
\end{aligned}
\tag{9}
$$

The following discussion explains how Eq. (8) can still enable the design of different types of rephasing by adjusting the value of Δt to obtain a final closed relative orbit around the along-track point y_{fd}, with desired relative eccentricity. These types of maneuvers may be envisioned for close approach to a target and fly around for monitoring purposes. It must be noted that Eq. (8) shows 2ω as the highest frequency. The Nyquist–Shannon sampling theorem presented in [16] can be used to determine how many points are needed to approximate the function in Eq. (8). By computing Eq. (8) at Δt points spaced by a $1/(4\omega)$ time distance, that is, theoretically 8π points total (i.e., at least 26), an entire orbital period is approximated. A desired e_{rel} value can be then interpolated using these points (e.g., using splines), posing minimal computational burden.

C. Analytical Solution for Initial Eccentric Orbit

The direct application of Eq. (3) on Eq. (1), starting from an eccentric orbit with the same semimajor axis of the LVLH orbit [i.e., $\boldsymbol{x}(t_0) = (\,x_0 \quad y_0 \quad \dot{x}_0 \quad -2\omega x_0\,)^T$] as described in [14], and considering a variable Δt, results in the following expression for the final state:

$$s=\sin(\dots)\qquad c=\cos(\dots)$$

$$x_f=x(t^*+2\Delta t)=\frac{1}{2\omega^2}\begin{bmatrix}2x_0\omega^2c(2\omega\Delta t+\alpha_3)-2\bar{u}s\left(\frac{1}{2}\alpha_3\right)+\bar{u}s(2\omega\Delta t+\alpha_3)+2\bar{u}s(\alpha_3+\omega\Delta t)+\\ -4\bar{u}s\left(\frac{1}{2}\alpha_3+\omega\Delta t\right)+\bar{u}s(2\omega\Delta t)+2\bar{u}s(\omega\Delta t)+\bar{u}s(\alpha_3)+\\ -2\bar{u}s\left(2\omega\Delta t+\frac{1}{2}\alpha_3\right)+2\dot{x}_0\omega s(2\omega\Delta t+\alpha_3)\end{bmatrix}$$

$$y_f=y(t^*+2\Delta t)=-2x_0\sin(2\omega\Delta t+\alpha_3)+\frac{1}{2\omega^2}\begin{bmatrix}4\dot{x}_0\omega c(2\omega\Delta t+\alpha_3)+2\bar{u}+2\bar{u}c(\alpha_3)+3\omega^2y_{\mathrm{fd}}-\omega^2y_0+\\ -4\bar{u}c\left(\frac{1}{2}\alpha_3\right)+4\bar{u}c(\alpha_3+\omega\Delta t)-4\bar{u}c\left(2\omega\Delta t+\frac{1}{2}\alpha_3\right)+\\ +2\bar{u}c(2\omega\Delta t+\alpha_3)-4\dot{x}_0\omega+2\bar{u}c(2\omega\Delta t)+\\ -8\bar{u}c\left(\frac{1}{2}\alpha_3+\omega\Delta t\right)+4\bar{u}c(\omega\Delta t)\end{bmatrix}$$

$$\dot{x}_f=\dot{x}(t^*+2\Delta t)=-\frac{1}{2\omega}\begin{bmatrix}2\omega^2x_0s(\alpha_3+2\omega\Delta t)+2\bar{u}c\left(\frac{1}{2}\alpha_3\right)-\bar{u}-\bar{u}c(\alpha_3+2\omega\Delta t)-\bar{u}c(2\omega\Delta t)+\\ +2\bar{u}c\left(\frac{1}{2}\alpha_3+2\omega\Delta t\right)-\bar{u}c(\alpha_3)+4\bar{u}c\left(\frac{1}{2}\alpha_3+\omega\Delta t\right)-2\bar{u}c(\omega\Delta t)+\\ -2\bar{u}c(\alpha_3+\omega\Delta t)-2\dot{x}_0\omega c(\alpha_3+2\omega\Delta t)\end{bmatrix}$$

$$\dot{y}_f=\dot{y}(t^*+2\Delta t)=-\frac{1}{\omega}\begin{bmatrix}2\dot{x}_0\omega s(\alpha_3+2\omega\Delta t)-2\bar{u}s\left(\frac{1}{2}\alpha_3\right)+2\bar{u}s(\alpha_3+\omega\Delta t)+\bar{u}s(\alpha_3)+\bar{u}s(\alpha_3+2\omega\Delta t)+\\ +2\bar{u}s(\omega\Delta t)-4\bar{u}s\left(\frac{1}{2}\alpha_3+\omega\Delta t\right)+2\omega^2x_0c(\alpha_3+2\omega\Delta t)+\bar{u}s(2\omega\Delta t)+\\ -2\bar{u}s\left(\frac{1}{2}\alpha_3+2\omega\Delta t\right)\end{bmatrix},\quad \alpha_3=\omega\sqrt{\frac{2(y_{\mathrm{fd}}-y_0)}{\bar{u}}} \tag{10}$$

As in the previous case, the condition $\dot{y}_f=-2\omega x_f$ is satisfied in Eq. (10). The center of the ellipse representing the final relative orbit, computed as in Eq. (5) using the solution (6) and Eq. (10) is obtained as

$$\bar{x}=0,\qquad \bar{y}=y_{\mathrm{fd}}-\frac{2}{\omega}\dot{x}_0 \tag{11}$$

Equation (11) shows that rephasing to a final equilibrium relative orbit, with the center at a desired location, is possible. In fact, starting from t_0, and waiting for any time instant when $\dot{x}=0$ (there are two positions along the closed relative orbit that correspond to this condition), the input-shaped control signal can be applied then. The wait time is given by

$$t_{\mathrm{wait}}=\frac{1}{\omega}\tan^{-1}\left(\frac{\dot{x}_0}{\omega x_0}\right)+k\pi,\qquad k=0,1,2,\dots \tag{12}$$

The relative eccentricity can only be maintained equal to the initial value or increased [Eq. (13)]. This increase, indicated with a Δ, once again, depends on the time interval Δt as follows:

Similar to Eqs. (8) and (13) can be analytically differentiated with respect to Δt, but in this case, the derivative is trivial to analyze and thus it is not shown for brevity. The behavior of the function in Eq. (13) does not show maximum and minimum values at times multiple (or submultiple) of the orbital period. The Nyquist–Shannon sampling theorem presented in [16] must be invoked again, to find the number of points to approximate the function in Eq. (13), and then interpolation can be used to compute the correct Δt for a desired Δe_{rel}.

III. Guidance Trajectories

This section presents the different types of trajectories that can be designed using input shaping. All the sample cases assume a low-thrust control acceleration of $2\mathrm{e}-5\ \mathrm{m/s^2}$. The amount of maximum acceleration should be varied depending on the actuators, affecting the duration of the maneuver [see Eq. (3)].

$$s=\sin(\dots),\quad c=\cos(\dots),\quad \Delta e_{\mathrm{rel}}=\frac{1}{2}\sqrt{\begin{matrix}\left[\begin{matrix}x_0\omega^2c\left(\frac{2}{3}\alpha_2+2\omega\Delta t\right)+\dot{x}_0\omega s\left(\frac{2}{3}\alpha_2+2\omega\Delta t\right)+\bar{u}s\left(\frac{2}{3}\alpha_2+\omega\Delta t\right)+\\ \frac{4}{\omega^4}\left[-\bar{u}s\left(\frac{1}{3}\alpha_2+2\omega\Delta t\right)-2\bar{u}s\left(\frac{1}{3}\alpha_2+\omega\Delta t\right)+\frac{1}{2}\bar{u}s\left(\frac{2}{3}\alpha_2+2\omega\Delta t\right)-\bar{u}s\left(\frac{1}{3}\alpha_2\right)+\right]+\\ +\frac{1}{2}\bar{u}s\left(\frac{2}{3}\alpha_2\right)+\frac{1}{2}\bar{u}s(2\omega\Delta t)+\bar{u}s(\omega\Delta t)\end{matrix}\right]^2\\ \left[\begin{matrix}-2x_0\omega^2s\left(\frac{2}{3}\alpha_2+2\omega\Delta t\right)+2\dot{x}_0\omega c\left(\frac{2}{3}\alpha_2+2\omega\Delta t\right)-4\bar{u}c\left(\frac{1}{3}\alpha_2+\omega\Delta t\right)+\\ +\frac{1}{\omega^4}\left[+2\bar{u}c\left(\frac{2}{3}\alpha_2+\omega\Delta t\right)-2\bar{u}c\left(\frac{1}{3}\alpha_2+2\omega\Delta t\right)+\bar{u}c\left(\frac{2}{3}\alpha_2+2\omega\Delta t\right)-2\bar{u}c\left(\frac{1}{3}\alpha_2\right)+\right]\\ +\bar{u}c\left(\frac{2}{3}\alpha_2\right)+2\bar{u}c(\omega\Delta t)+\bar{u}c(2\omega\Delta t)+\bar{u}\end{matrix}\right]^2\end{matrix}}$$

$$\alpha_2=\omega\sqrt{\frac{3y_{\mathrm{fd}}-3y_0}{\bar{u}}} \tag{13}$$

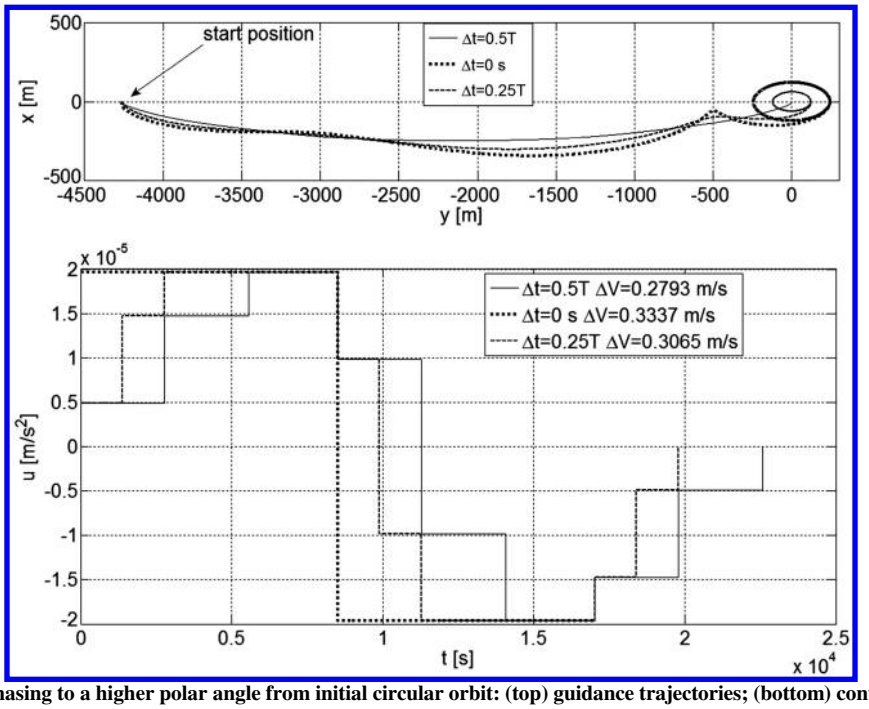

Fig. 1 Rephasing to a higher polar angle from initial circular orbit: (top) guidance trajectories; (bottom) control profiles.

A. Initial Circular Orbit

The first example is a forward rephasing maneuver, increasing the polar angle of 0.036 deg, in a circular orbit of radius 6778.1 km. In the linear approximation of the LVLH frame, this can be set up as starting from $\boldsymbol{x}(t_0) = 10^3[0 \quad -4.2588 \quad 0 \quad 0]^T$, with units in meters and meters per second, and targeting the origin.

Figure 1 shows the guidance trajectories for three different values of Δt. For $\Delta t = 0.5T$, there is no residual oscillation at the target point. The maximum relative eccentricity is obtained for $\Delta t = 0$, whereas $\Delta t = 0.25T$ is an example of intermediate relative eccentricity [see Eq. (8)]. The ΔVs are also shown; for the case of $\Delta t = 0.5T$, a comparison with a two-impulse maneuver can be straightforwardly made (see [17]). The impulsive ΔV is 0.1326 m/s^2. The cost of continuous thrust schemes is expected to be higher in terms of ΔV, but lower in terms of propellant consumption, because low-thrust continuous engines can be very efficient compared with impulsive ones.

The control profiles shown in the bottom plot of Fig. 1 may be straightforwardly tracked by single thrust, on–off, continuous low-thrust engines, by means of pulse width modulation, or followed with engine systems capable of generating a limited set of thrust values, as described in [3].

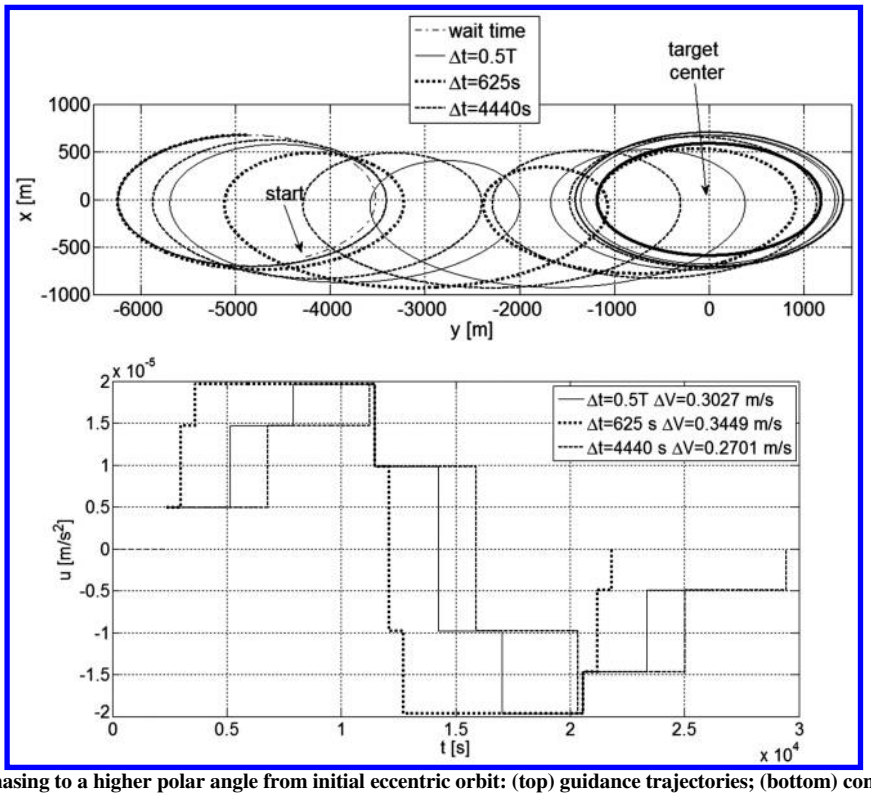

Fig. 2 Rephasing to a higher polar angle from initial eccentric orbit: (top) guidance trajectories; (bottom) control profiles.

B. Initial Eccentric Orbit

The second example targets the same rephasing angle and semimajor axis, but the spacecraft possesses an initial eccentricity of 0.0001. In the linear approximation of the LVLH frame, this can be set up as starting from $\boldsymbol{x}(t_0) = 10^3[-0.6043 \quad -4.2584 \quad 0.0004 \quad -2\omega x_0]^T$, with units in meters and meters per second, and targeting the origin. A waiting time (coasting) is used [Eq. (12)], with $k = 0$, before applying the control signal. Figure 2 shows the guidance trajectories for three different values of Δt. For $\Delta t = 0.5T$, an intermediate relative eccentricity is obtained (between initial and maximum achievable) on the final relative orbit. For $\Delta t = 625s$, the minimum relative eccentricity is obtained. Finally, for $\Delta t = 4440s$, the maximum relative eccentricity is obtained. These Δt values are obtained analyzing Eq. (13) through the procedure outlined in the preceding section.

As commented in the preceding case, the control profiles shown in the bottom plot of Fig. 2 can be tracked by engine systems as those described in [3].

It is important to underline once again that the illustrated guidance solutions are valid in the simplified linear dynamics case with relatively small distances involved. To implement these solutions on a real spacecraft, a closed-loop controller is needed, to track the analytical guidance profiles.

IV. Conclusions

This Note introduced novel analytical guidance solutions for spacecraft rephasing maneuvers, based on linearized equations of spacecraft relative motion and a technique known as input shaping. Input shaping is proposed for the first time in spacecraft orbital maneuvering. Thanks to the technique proposed, realistic finite magnitude and finite duration along-track-only control can be considered. The analytical solutions can lead a spacecraft from an initial location along the orbit to a desired final location on the same course, as well as modify its path so that it will fly in an equilibrium fashion about a desired point ahead or behind its initial location. The guidance is presented in close-form solutions and graphically illustrated in this Note with a few examples. Procedures to choose key guidance parameters affecting the size of the final relative motion are also provided. The proposed guidance could be used for real missions, when combined with an appropriate feedback control technique.

Acknowledgment

The author wishes to thank the U.S. Air Force Office of Scientific Research for sponsoring this investigation under the Young Investigator Program (award FA9550-12-1-0072).

References

[1] Kumar, K. D., Bang, H. C., and Tahk, M. J., "Satellite Formation Flying Using Along-Track Thrust," *Acta Astronautica*, Vol. 61, Nos. 7–8, 2007, pp. 553–564. doi:10.1016/j.actaastro.2007.01.069

[2] Starin, R. S., Yedavalli, R. K., and Sparks, A. G., "Spacecraft Formation Flying Maneuvers Using Linear-Quadratic Regulation with no Radial Axis Input," *AIAA Guidance, Navigation, and Control Conference and Exhibit*, AIAA Paper 2001-4029, 2001.

[3] Bevilacqua, R., and Romano, M., "Fuel-Optimal Spacecraft Rendezvous with Hybrid On–Off Continuous and Impulsive Thrust," *Journal of Guidance, Control, and Dynamics*, Vol. 30, No. 4, 2007, pp. 1175–1178. doi:10.2514/1.27716

[4] Burges, J. D., Hall, M. J., and Lightsey, E. G., "Evaluation of a Dual-Fluid Cold-Gas Thruster Concept," *International Journal of Mechanical and Aerospace Engineering*, Vol. 6, 2012, pp. 232–237.

[5] Banerjee, A., Pedreiro, N., and Singhose, W., "Vibration Reduction for Flexible Spacecraft Following Momentum Dumping With/Without Slewing," *Journal of Guidance, Control, and Dynamics*, Vol. 24, No. 3, 2001, pp. 417–428.

[6] Cutforth, C. F., and Pao, L. Y., "Adaptive Input Shaping for Maneuvering Flexible Structures," *Automatica*, Vol. 40, No. 4, 2004, pp. 685–693. doi:10.1016/j.automatica.2003.11.013

[7] Pao, L. Y., "Analysis of the Frequency, Damping, and Total Insensitivities of Input Shaping Designs," *Journal of Guidance, Control, and Dynamics*, Vol. 20, No. 5, 1997, pp. 909–915. doi:10.2514/2.4134

[8] Baumgart, M. D., and Pao, L. Y., "Discrete Time-Optimal Command Shaping," *Automatica*, Vol. 43, No. 8, 2007, pp. 1403–1409. doi:10.1016/j.automatica.2007.01.003

[9] Lau, M. A., and Pao, L. Y., "Input Shaping and Time-Optimal Control of Flexible Structures," *Automatica*, Vol. 39, No. 5, 2003, pp. 893–900.

[10] Pao, L. Y., and Cutforth, C. F., "On Frequency-Domain and Time-Domain Input Shaping for Multi-Mode Flexible Structures," *Journal of Dynamic Systems, Measurement, and Control*, Vol. 125, No. 3, 2003, pp. 494–497. doi:10.1115/1.1591808

[11] Pao, L. Y., and Lau, M. A., "Expected Residual Vibration of Traditional and Hybrid Input Shaping Designs," *Journal of Guidance, Control, and Dynamics*, Vol. 22, No. 1, 1998, pp. 162–165.

[12] Romano, M., Agrawal, B. N., and Bernelli-Zazzera, F., "Experiments on Command Shaping Control of a Manipulator with Flexible Links," *Journal of Guidance, Control, and Dynamics*, Vol. 25, No. 2, 2002, pp. 232–239. doi:10.2514/2.4903

[13] Hill, G., "Researches in Lunar Theory," *American Journal of Mathematics*, Vol. 1, No. 1, 1878, pp. 5–26. doi:10.2307/2369430

[14] Clohessy, W. H., and Wiltshire, R. S., "Terminal Guidance System for Satellite Rendezvous," *Journal of Aerospace Sciences*, Vol. 27, No. 9, Sept. 1960, pp. 653–658.

[15] Leonard, C. L., Hollister, W. M., and Bergmann, E. V., "Orbital Formationkeeping with Differential Drag," *Journal of Guidance, Control, and Dynamics*, Vol. 12, No. 1, 1989, pp. 108–113. doi:10.2514/3.20374

[16] Shannon, C. E., "Communication in the Presence of Noise," *Proceedings of the Institute of Radio Engineers*, Vol. 37, No. 1, Jan. 1949, pp. 10–21; reprint *Proceedings of the IEEE*, Vol. 86, No. 2, Feb. 1998, pp. 447–457.

[17] Doll, J. R., and Gobetz, F. W., "Survey of Impulsive Trajectories," *AIAA Journal*, Vol. 7, No. 5, 1969, pp. 801–834. doi:10.2514/3.5231

This article has been cited by:

1. David Guglielmo, Sanny Omar, Riccardo Bevilacqua, Laurence Fineberg, Justin Treptow, Bradley Poffenberger, Yusef Johnson. 2019. Drag Deorbit Device: A New Standard Reentry Actuator for CubeSats. *Journal of Spacecraft and Rockets* **56**:1, 129-145. [Abstract] [Full Text] [PDF] [PDF Plus]
2. Margaret Lawn, Giuseppe Di Mauro, Riccardo Bevilacqua. 2018. Guidance Solutions for Spacecraft Planar Rephasing and Rendezvous Using Input Shaping. *Journal of Guidance, Control, and Dynamics* **41**:1, 255-267. [Citation] [Full Text] [PDF] [PDF Plus]
3. Gang Zhang, Dong Ye. 2017. Optimal short-range rendezvous using on–off constant thrust. *Aerospace Science and Technology* **69**, 209-217. [Crossref]
4. Juan L. Gonzalo, Claudio Bombardelli. 2017. Optimal Continuous-Thrust Rephasing Maneuver in Circular Orbit. *Journal of Guidance, Control, and Dynamics* **40**:5, 1155-1165. [Abstract] [Full Text] [PDF] [PDF Plus]
5. David Guglielmo, David Pérez, Riccardo Bevilacqua, Leonel Mazal. 2016. Spacecraft relative guidance via spatio-temporal resolution in atmospheric density forecasting. *Acta Astronautica* **129**, 32-43. [Crossref]
6. David Pérez, Riccardo Bevilacqua. 2016. Differential Drag-Based Reference Trajectories for Spacecraft Relative Maneuvering Using Density Forecast. *Journal of Spacecraft and Rockets* **53**:1, 234-239. [Citation] [Full Text] [PDF] [PDF Plus]
7. Gang Zhang, Guangfu Ma, Dongbai Li. 2015. Two-impulse transfer between coplanar elliptic orbits using along-track thrust. *Celestial Mechanics and Dynamical Astronomy* **121**:3, 261-274. [Crossref]
8. David Pérez, Riccardo Bevilacqua. 2014. Lyapunov-Based Adaptive Feedback for Spacecraft Planar Relative Maneuvering via Differential Drag. *Journal of Guidance, Control, and Dynamics* **37**:5, 1678-1684. [Citation] [Full Text] [PDF] [PDF Plus]
9. Riccardo Bevilacqua, Thomas Alan Lovell. 2014. Analytical guidance for spacecraft relative motion under constant thrust using relative orbit Elements. *Acta Astronautica* . [Crossref]